Effect of the Nuclear Equation of State and Relativistic Turbulence on Core-Collapse Supernovae

Luca Boccioli[1,*], *Grant* Mathews[1], and *Evan* O'Connor[2]

[1]Center for Astrophysics, Department of Physics & Astronomy, University of Notre Dame, 225 Nieuwland Science Hall, Notre Dame, IN 46556, USA

[2]The Oskar Klein Centre, Department of Astronomy, Stockholm University, AlbaNova, SE-106 91 Stockholm, Sweden

Abstract. The nuclear Equation of State (EoS) is an important component in the evolution and subsequent explosion of core collapse supernovae. We make a survey of various equations of state that can be found in the literature and analyze their effect on the explosion. To simulate the supernovae, we use the general relativistic spherically-symmetric code GR1D, modified to take into account the effects of three-dimensional turbulence through a new mixing length theory approach (STIR). We show that the viability of the explosion is quite EoS dependent and that the strength of explosions correlate best with the central entropy density right after bounce and the onset of turbulent mixing in the proto-neutron star.

1 Introduction

Core-collapse supernovae have been one of the main focuses of computational astrophysics for more than 50 years. The tremendous advance in CPU technology enabled very detailed three-dimensional simulations to be developed, which greatly improved our knowledge of the explosion mechanism, but there are still many challenges left. One of the main uncertainties affecting the physics of supernovae is the Equation of State (EOS) of nuclear matter. Core-collapse supernovae generate thermodynamic conditions that can go from very low densities in the mantle (10^3 g cm^{-3}) to very high densities in the core (10^{15} g cm^{-3}) as well as all the values in between. At the same time, temperatures can also vary from 1 MeV to 100 MeV, while electron fractions can be as low as ~ 0.01 and as large as ~ 0.6. To adequately describe the explosion, a detailed knowledge of the EOS of matter across all these thermodynamic regimes is required. However, at high densities the EOS is still poorly constrained, especially when considering finite temperature effects [1–4].

Other important challenges that need to be addressed concern neutrinos and their interactions with matter. It is now quite well established that neutrino-delayed heating [5] is the main mechanism responsible for the explosion of massive stars. Therefore, a detailed knowledge of the thermodynamic dependence of neutrino-matter interactions, alongside realistic algorithms that describe the transport of neutrinos across the star, are required [6–8]. In this proceeding, however, we will only focus on the EOS.

*e-mail: lbocciol@nd.edu

EOS	Type	n_0 (fm^{-3})	J (MeV baryon^{-1})	K_0 (MeV baryon^{-1})	m_n^*/m_n -	M_{max} $M_\odot$
SFHo	RMF	0.1583	31.57	245.40	0.7608	2.05
DD2	RMF	0.1491	32.73	242.70	0.5625	2.14
HShen	RMF	0.1455	36.95	281.00	0.6340	2.21
LS220	SRO	0.1549	28.61	219.85	1.0000	2.04
APR	SRO	0.1600	32.59	266.00	0.6985	2.19
KDE0v1	SRO	0.1646	34.58	227.53	0.7442	1.97
SLy4	SRO	0.1595	32.00	229.90	0.6952	2.05

Table 1. The different columns represent the nuclear saturation density (n_0) the symmetry energy at saturation density (J), the nuclear incompressibility (K_0), the nucleon effective mass (m_n^*) and the maximum mass of a neutron star (M_{max}). The first four equations of state are calculated using RMF theory, while the last three were generated using the SRO code from [31].

In this work, we use the spherically symmetric model in full general relativity described in [9] to study the impact of the EOS on the explosion. This model can achieve an explosion by means of the inclusion of turbulent convection using Mixing-Length Theory (MLT). Specifically, it is a general relativistic version of STIR, first developed by [10]. In the past, several studies were carried out, analyzing the effect of the EOS on the dynamics of CCSNe (e.g. [11–29]). Here, we employ 7 different EOS, based on different microscopic models, and with those simulate four different progenitor models.

Our work was inspired by two recent papers [26, 28], that study the effect of the EOS on the structure of the PNS and on the explosion. Both papers focus on EOSs that were calculated using Skyrme energy density functionals, whereas our study also includes EOSs generated using Relativistic Mean Field (RMF) models. In these two studies, by varying several Skyrme parameters, they observed that the effective nucleon mass m_n^* is the parameter that best correlates with the strength of the explosion. In this work, however, we will study how EOSs generated using different microscopical theories affect the explosion. Natural units will be adopted throughout the manuscript, i.e. $G = c = M_\odot = 1$.

2 Methods

2.1 Nuclear Equations of State

We used 7 different EOS to simulate 4 different progenitors with masses of 9, 15, 20 and 25 $M_\odot$ from [30]. The EOS we chose are listed in table 1. In previous studies [26, 28] some of the nuclear parameters that can more significantly impact the explosion have been identified. In particular, the effective nucleon mass in symmetric matter at saturation density m_n^* was found to be the one that best correlates with the strength of the explosion. The details of the EOSs used in this study is summarized below:

- The SFHo and DD2 EOSs are taken from [32], which uses a Relativistic Mean Field (RMF) approach, with the parametrization of nucleon interactions from [15] and [33], respectively. Nuclei near saturation density are treated using an NSE approach, with several thousands nuclei taken into account.

- The HShen EOS from [34] is based on RMF theory. The difference with the SFHo and DD2 EOS is that the HShen uses the Single Nucleus Approximation (SNA), based upon a Thomas-Fermi model, to describe nuclei near nuclear saturation density.
- The APR EOS [35, 36]: At high densities it uses realistic nuclear potentials resulting from fits to nucleon-nucleon scattering. It also includes a phase transition to a neutral pion condensate. It is then connected to a network of ∼3300 nuclei in Nuclear Statistical Equilibrium (NSE) at low densities using the SRO code [31].
- The LS220 [11], KDE0v1 [37] and SLy4 [38]: These are based on Skyrme parameterizations as described in [31]. Additionally, nuclei at densities near nuclear saturation density are described using the compressible liquid drop theory, in the same fashion as [11]. These EOS are then connected to a network of ∼3300 nuclei in Nuclear Statistical Equilibrium (NSE) at low densities using the SRO code [31].

The last four EOSs were taken from the SROEOS code of [31]. Hence, at densities below nuclear saturation density, they are described using a compressible liquid-drop model at finite temperature in which heavy nuclei are described using SNA. We therefore divide these EOSs in two categories: RMF-type (the first three) and SRO-type (the last four). The gravitational mass versus radius relationships for cold neutron can be seen in Figure 1, together with some observational constraints on the mass and radius of Neutron Stars. Despite the fact that some of them are not consistent with observation constraints, these EOSs represent a reasonable catalogue of possible equations of state.

2.2 Supernova model

One of the mechanisms that can more significantly impact the delayed-neutrino heating mechanism is neutrino-driven turbulent convection, as many previous studies have shown [46–49]. The reason is that material behind the expanding shock is heated by neutrinos escaping the proto-neutron star, and turbulent convection can increase the time spent by the material in the gain region, increasing the probability of interaction with neutrinos. Hence, neutrino-driven turbulence is a key component of the explosion mechanism of supernovae.

To analyze how different EOSs affect the explosion, we use the model described in [9], which uses a general relativistic version STIR [10] to include neutrino-driven turbulent convection in the spherically symmetric code `GR1D`. STIR includes the effects of turbulent convection in spherically symmetric simulations using a time-dependent Mixing-Length Theory (MLT) approach. The energy coming from turbulent convection can therefore trigger an explosion even in spherically symmetric simulations. We now briefly summarize the main features of STIR, but more details can be found in [49], [10] and [9]. The metric used in `GR1D` is:

$$\begin{aligned} ds^2 &= g_{\mu\nu}x^\mu x^\nu \\ &= -\alpha(r,t)^2dt^2 + X(r,t)^2dr^2 + r^2d\Omega^2 \,, \end{aligned} \tag{1}$$

where α is the lapse function and X is a function of the gravitational mass at radius r.

STIR adds an extra equation to the standard hydrodynamic ones solved in `GR1D`, to account for the time evolution of the turbulent energy:

$$\begin{aligned} &\frac{\partial D v_{\rm turb}^2}{\partial t} + \frac{1}{r^2}\frac{\partial}{\partial r}[\frac{\alpha r^2}{X} D(v_{\rm turb}^2 v - D_{\rm K}\nabla v_{\rm turb}^2)] \\ &= -\alpha X\left(\rho v_{\rm turb}^2 \frac{\partial v}{\partial r} + \rho v_{\rm turb}\omega_{\rm BV}^2\Lambda_{\rm mix} - \rho\frac{v_{\rm turb}^3}{\Lambda_{\rm mix}}\right) , \end{aligned} \tag{2}$$

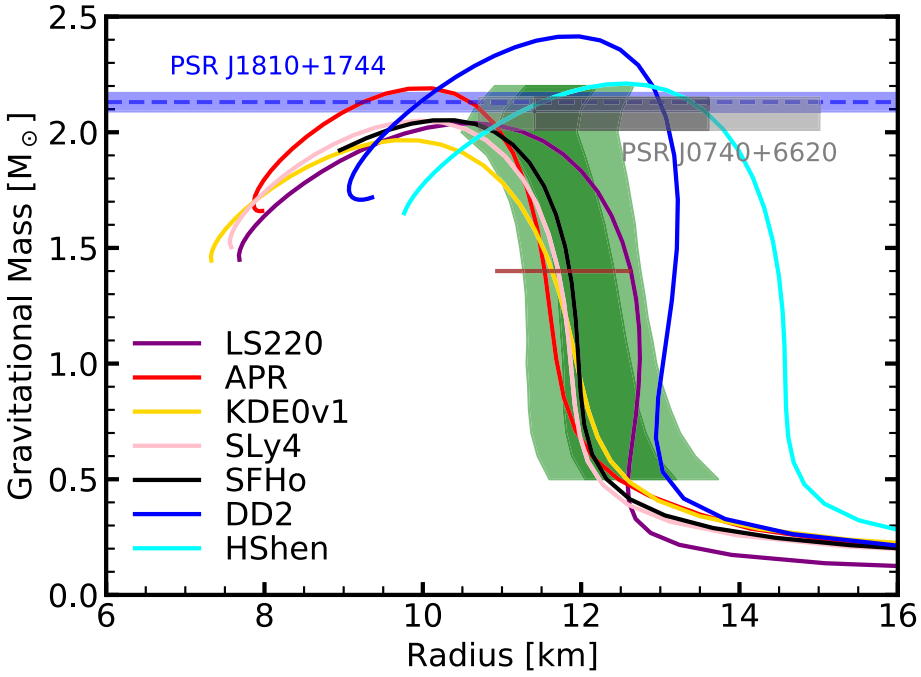

Figure 1. Gravitational mass vs radius, from the various equations of state adopted in the present work. The green shaded region shows the NS mass-radius constraints from model A of [39]. The grey band represents the mass and radius of the millisecond pulsar PSR J0740+6620. The mass has been measured by [40] and [41], with a value of 2.08 ± 0.07 $M_\odot$. The radius has been independently estimated by [42] and [43] using NICER data. Here we show the latter, where the lighter grey region represents a 95% confidence level, corresponding to a radius of $12.39^{+2.63}_{-1.68}$ km, while the darker region shows the 1σ confidence level, corresponding to a radius of $12.39^{+1.30}_{-0.98}$ km. The blue dotted line is the mass of PSR J1810+1744 measured by [44], and the shaded blue region represents the 1σ confidence level. The brown horizontal band shows the constraint on the radius of a 1.4 $M_\odot$ neutron star from [45].

where $D = X\rho W$ is the conserved density, $W = (1 - v^2)^{-1/2}$ is the Lorentz factor and $v_{\rm turb}$ is the turbulent velocity. The velocity is defined as $v = Xv^r$, where v_r is the coordinate velocity. Finally, $D_{\rm K} = \alpha_{\rm K} v_{\rm turb} \Lambda_{\rm mix}$ is the diffusion coefficient. The most important quantities of this model are the mixing length

$$\Lambda_{\rm mix} = \alpha_{\rm MLT} \frac{P}{\rho \, {\rm d}\phi/{\rm d}r} \, , \tag{3}$$

and the Brunt-Väisälä frequency

$$\omega^2_{\rm BV} = \frac{\alpha^2}{\rho h X^2} \left(\frac{{\rm d}\phi}{{\rm d}r} - v \frac{\partial v}{\partial r} \right) \left(\frac{\partial \rho (1+\epsilon)}{\partial r} - \frac{1}{c_s^2} \frac{\partial P}{\partial r} \right) , \tag{4}$$

where $\phi = \ln \alpha$ reduces to the Newtonian potential in the non-relativistic limit and c_s is the sound speed. The quantity $h = 1 + \epsilon + P/\rho$ represents the relativistic enthalpy, where P is the pressure and ϵ is the internal energy.

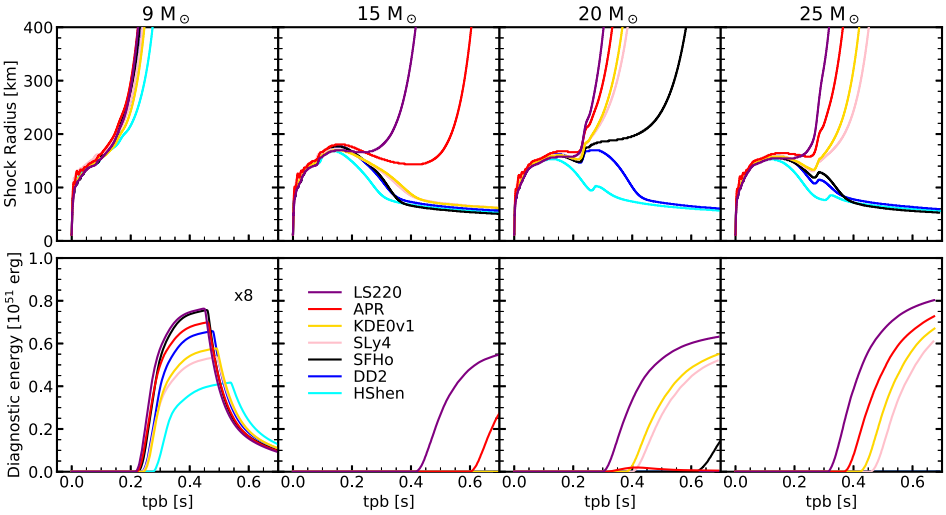

Figure 2. The upper panels display shock radius vs time for different progenitors and EOSs, while the lower panels display the diagnostic energy vs time. Notice that for the 9 $M_\odot$ progenitor the diagnostic energies have been multiplied by a factor of 8 so that they could be more clearly shown on the same scale used for the other progenitors.

The parameters controlling the strength of the explosion are: $\alpha_{\rm MLT}$ and $\alpha_{\rm K}$. The first one controls the magnitude of the mixing length, whereas the second one controls the magnitude of the diffusion coefficients $D_{\rm K}$. We have not shown all the hydrodynamic equations here, but it's important to point out that other diffusion coefficients, analogous to $D_{\rm K}$, are added to the evolution equations for neutrino energy density, internal energy and electron fraction. The total number of parameters in the model is therefore 5. However, we fix $\alpha_{\rm K}$ and the other parameters governing diffusion to 1/6, consistently with the choices of [50] and [10]. The only parameter we vary is $\alpha_{\rm MLT}$.

The simulations carried out for this work were run using a modified version of `GR1D` [51, 52], which is based on spherically symmetric hydrodynamics and radiation transport in full General Relativity (GR). Neutrino opacitiy tables were generated using the open-source code `NuLib` [52].

3 Results

Given the high densities reached inside the PNS, the dynamics of supernovae can be greatly impacted by the EOS. To illustrate this, we show some of the most significant thermodynamic quantities at the center of the PNS in Figure 3, for different progenitors and EOSs. As one can clearly see, central density and temperature can vary significantly as a function of EOS, but they do not correlate with the strength of explosion. On the contrary, the central entropy in the first 50 ms after bounce correlates extremely well with the strength of the explosion, even though the range spanned by different EOSs is not as large as for the other two quantities. One can then conclude that the hierarchy of central entropies follows the hierarchy of explosion strength, with the only exception of the SLy4 and KDE0v1 EOSs, which will be discussed below.

A similar correlation was found by the studies of [26] and [28]. In both papers, they only focused on one type of EOS which, at high densities, is based on Skyrme interactions between nucleons. By doing this, they were able to vary different nuclear parameters — such as the effective mass, the symmetry energy, the incompressibility and others — while keeping all the other ones fixed. This approach allowed them to observe the impact of different properties of the EOS on the explosion. Both analyses revealed that the quantity responsible for the greatest change in PNS structure is the effective mass of nuclei at saturation density m_n^*. This translates into a change in the dynamics of explosion, which depends on how fast the PNS contraction is [28], since it changes the location and thermodynamic properties of the neutrinospheres for all flavors [26]. As a side note, they also pointed out that a change in the effective mass corresponds to a change in the central entropy: larger effective masses lead to larger central entropies.

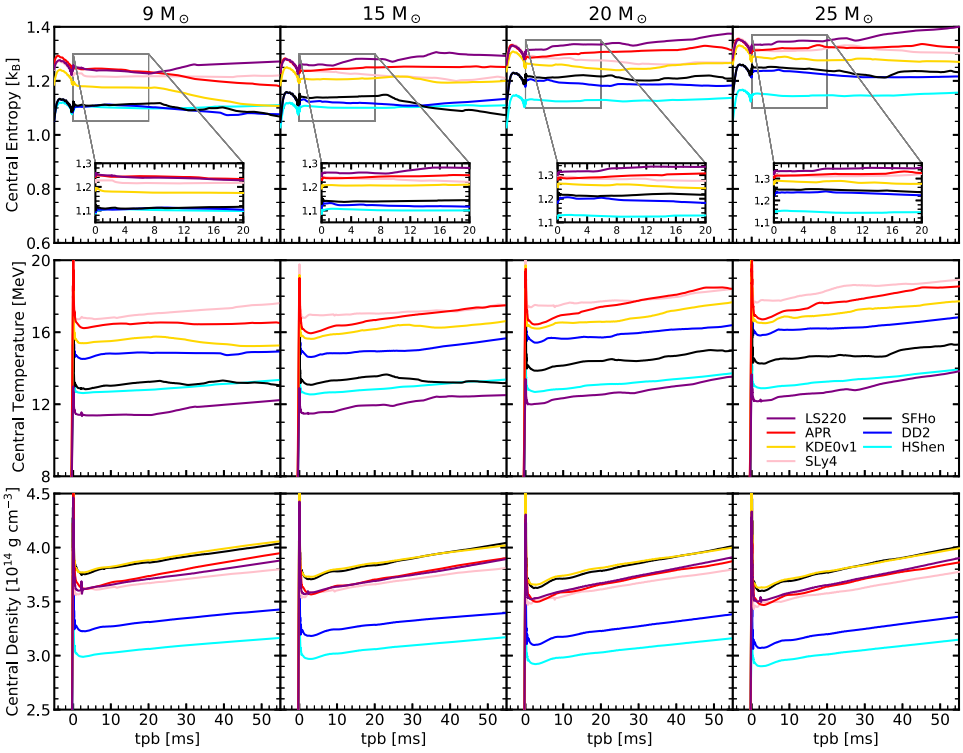

Figure 3. The first three rows show the main central thermodynamic variables for different progenitors (columns) and EOSs (colors) as a function of time post bounce. The last row shows the ratio of the nucleon effective mass to the nucleon mass calculated for the central values of densities and temperatures as a function of time post bounce. The central entropy at early times tpb $\lesssim$ 5 ms is larger for EOSs that yield stronger explosions. See the text for a more detailed discussion.

We complement these studies by including not only EOSs based on Skyrme interactions, such as the LS220, KDE0v1, and SLy4, but also the APR EOS as well as EOSs based on RMF theory. Since the finite-temperature part of the APR EOS was constructed using the SRO-code [31], which was also used to generate the Skyrme-type EOSs, they share the same

properties near saturation density. Hence, we consider them to be "SRO-type". The difference between the APR and the Skyrme-type EOSs is that the nuclear potentials for the Skyrme-type EOSs are derived from the energy density of nuclear matter, whereas for the APR they are derived from nucleon-nucleon scattering. The EOSs calculated using RMF theory are the SFHo, DD2 and HShen. The first two use an NSE treatment of nuclei near saturation density, and the HShen uses a Thomas-Fermi description of nuclei instead. In the following paragraphs we will investigate the differences among these frameworks used to calculate the nuclear EOS.

We begin our analysis by comparing the EOSs calculated using Skyrme interactions (i.e. LS220, KDE0v1 and SLy4). One can easily notice that the effective mass correlates with the strength of explosion. If however one compares all of the EOSs considered in this study, this correlation breaks down. Also, despite the fact that the APR uses the same treatment of nuclei near saturation density as the Skyrme-type EOSs, it does not follow the correlation between strength of explosion and effective mass. This, however, is not completely unexpected since the effective mass in the APR EOS has a more complicated density dependence [36]. Overall, this shows that the effective mass is not the only parameter that affects the strength of explosion. Interestingly, the only quantity that correlates with the strength of the explosion, regardless of the framework used to calculate the nuclear EOS, is the central entropy.

As mentioned above, KDE0v1 and SLy4 don't follow this correlation between strength of explosion and central entropy. From Figure 2, one can see that shock trajectories and explosion energies for these two EOSs are very similar across progenitors, with KDE0v1 yielding slightly stronger explosions. From the top panel of Figure 3, however, one can see that KDE0v1 gives a slightly smaller central entropy than SLy4. Hence, this shows that nuclear parameters other than m_n^* can also change the dynamics of the explosion. This can be seen by considering a Fermi liquid theory, in which the central entropy is given by $S_c \sim m_n^* T_c/\rho_c^{2/3}$ [53], where ρ_c, T_c and S_c are the central density, temperature and entropy, respectively. KDE0v1 has a larger saturation density, which increases the central density, and therefore lowers the central entropy. At the same time, it has a larger nucleon effective mass m_n^*, which increases the central entropy. These two competing effects slightly disrupt the hierarchy of central entropy. However, in this study the EOSs differ for several nuclear parameters, and therefore one doesn't expect a perfect correlation.

4 Conclusions

In this proceeding we have shown how the EOS affects the explosion of CCSNe using spherically symmetric, general relativistic simulations with a parametric treatment of turbulent convection.

We highlight a remarkable correlation between the central entropy immediately after bounce the strength of the explosion. This is in agreement with previous studies by [26] and [28], carried out by considering only Skyrme-type EOSs. In these works, they concluded that the effective nucleon mass is the nuclear parameter that most strongly correlates with the explosion. Our results using the three Skyrme EOSs considered in this work confirm this.

In addition to Skyrme-type EOSs we have also taken into account the APR EOS and three RMF-type EOSs. This breaks down the correlation between strength of explosion and effective nucleon mass. Because of that, the correlation between effective nucleon mass and central entropy reported in those studies [26, 28] is also no longer present in our simulations. However, we do obtain a remarkable correlation between central entropy and strength of the explosion. One can therefore conclude that the central entropy immediately after bounce is the best indicator of explodability, and it therefore plays an important role in determining the strength of the explosion. Finally, since SRO-type and RMF-type EOSs do not follow

the same correlation between effective mass and strength of explosion, we conclude that the approach used to calculate the EOS, and more specifically the treatment of nuclear matter near saturation density, has a significant impact on the explosion of CCSNe.

Acknowledgments

The authors would like to thank Andre da Silva Schneider for his help in calculating the symmetry energy of the EOSs adopted. Work at the University of Notre Dame supported by the U.S. Department of Energy under Nuclear Theory Grant DE-FG02-95-ER40934. EOC would like to acknowledge Vetenskapsrådet (the Swedish Research Council) for supporting this work under award numbers 2018-04575 and 2020-00452.

References

[1] T. Klähn, D. Blaschke, S. Typel, E.N.E. van Dalen, A. Faessler, C. Fuchs, T. Gaitanos, H. Grigorian, A. Ho, E.E. Kolomeitsev et al., PhRvC **74**, 035802 (2006)
[2] K. Hebeler, J.M. Lattimer, C.J. Pethick, A. Schwenk, ApJ **773**, 11 (2013), 1303.4662
[3] N.B. Zhang, B.A. Li, J. Xu, ApJ **859**, 90 (2018), 1801.06855
[4] G.F. Burgio, H.J. Schulze, I. Vidaña, J.B. Wei, Progress in Particle and Nuclear Physics **120**, 103879 (2021), 2105.03747
[5] H.A. Bethe, J.R. Wilson, ApJ **295**, 14 (1985)
[6] M. Liebendörfer, M. Rampp, H.T. Janka, A. Mezzacappa, ApJ **620**, 840 (2005), astro-ph/0310662
[7] C. Kato, H. Nagakura, Y. Hori, S. Yamada, ApJ **897**, 43 (2020), 2001.11148
[8] A. Mezzacappa, E. Endeve, O.E.B. Messer, S.W. Bruenn, Living Reviews in Computational Astrophysics **6**, 4 (2020), 2010.09013
[9] L. Boccioli, G.J. Mathews, E.P. O'Connor, ApJ **912**, 29 (2021), 2102.06767
[10] S.M. Couch, M.L. Warren, E.P. O'Connor, The Astrophysical Journal **890**, 127 (2020)
[11] J.M. Lattimer, D.F. Swesty, NuPhA **535**, 331 (1991)
[12] E. O'Connor, C.D. Ott, ApJ **730**, 70 (2011), 1010.5550
[13] M. Hempel, T. Fischer, J. Schaffner-Bielich, M. Liebendörfer, ApJ **748**, 70 (2012), 1108.0848
[14] H.T. Janka, Annual Review of Nuclear and Particle Science **62**, 407 (2012), 1206.2503
[15] A.W. Steiner, M. Hempel, T. Fischer, ApJ **774**, 17 (2013), 1207.2184
[16] S.M. Couch, ApJ **765**, 29 (2013), 1206.4724
[17] Y. Suwa, T. Takiwaki, K. Kotake, T. Fischer, M. Liebendörfer, K. Sato, ApJ **764**, 99 (2013), 1206.6101
[18] T. Fischer, M. Hempel, I. Sagert, Y. Suwa, J. Schaffner-Bielich, European Physical Journal A **50**, 46 (2014), 1307.6190
[19] P. Char, S. Banik, D. Bandyopadhyay, ApJ **809**, 116 (2015), 1508.01854
[20] J.P. Olson, M. Warren, M. Meixner, G.J. Mathews, N.Q. Lan, H.E. Dalhed, arXiv e-prints arXiv:1612.08992 (2016), 1612.08992
[21] S. Furusawa, H. Togashi, H. Nagakura, K. Sumiyoshi, S. Yamada, H. Suzuki, M. Takano, Journal of Physics G Nuclear Physics **44**, 094001 (2017), 1707.06410
[22] S. Richers, C.D. Ott, E. Abdikamalov, E. O'Connor, C. Sullivan, PhRvD **95**, 063019 (2017), 1701.02752
[23] H. Nagakura, W. Iwakami, S. Furusawa, H. Okawa, A. Harada, K. Sumiyoshi, S. Yamada, H. Matsufuru, A. Imakura, ApJ **854**, 136 (2018), 1702.01752

[24] V. Morozova, D. Radice, A. Burrows, D. Vartanyan, ApJ **861**, 10 (2018), 1801.01914
[25] A. Burrows, D. Vartanyan, J.C. Dolence, M.A. Skinner, D. Radice, SSRv **214**, 33 (2018), 1611.05859
[26] A.S. Schneider, L.F. Roberts, C.D. Ott, E. O'Connor, Phys. Rev. C **100**, 055802 (2019)
[27] A. Harada, H. Nagakura, W. Iwakami, H. Okawa, S. Furusawa, K. Sumiyoshi, H. Matsufuru, S. Yamada, ApJ **902**, 150 (2020), 2003.08630
[28] H. Yasin, S. Schäfer, A. Arcones, A. Schwenk, PhRvL **124**, 092701 (2020)
[29] S. Ghosh, N. Wolfe, C. Fröhlich, arXiv e-prints arXiv:2107.13016 (2021), 2107.13016
[30] T. Sukhbold, T. Ertl, S.E. Woosley, J.M. Brown, H.T. Janka, The Astrophysical Journal **821**, 38 (2016)
[31] A.S. Schneider, L.F. Roberts, C.D. Ott, Phys. Rev. C **96**, 065802 (2017)
[32] M. Hempel, J. Schaffner-Bielich, NuPhA **837**, 210 (2010), 0911.4073
[33] S. Typel, G. Röpke, T. Klähn, D. Blaschke, H.H. Wolter, PhRvC **81**, 015803 (2010), 0908.2344
[34] H. Shen, H. Toki, K. Oyamatsu, K. Sumiyoshi, ApJS **197**, 20 (2011), 1105.1666
[35] A. Akmal, V.R. Pandharipande, D.G. Ravenhall, PhRvC **58**, 1804 (1998), nucl-th/9804027
[36] A.S. Schneider, C. Constantinou, B. Muccioli, M. Prakash, PhRvC **100**, 025803 (2019), 1901.09652
[37] B.K. Agrawal, S. Shlomo, V.K. Au, PhRvC **72**, 014310 (2005), nucl-th/0505071
[38] E. Chabanat, P. Bonche, P. Haensel, J. Meyer, R. Schaeffer, NuPhA **627**, 710 (1997)
[39] J. Nättilä, A.W. Steiner, J.J.E. Kajava, V.F. Suleimanov, J. Poutanen, A&A **591**, A25 (2016), 1509.06561
[40] H.T. Cromartie, E. Fonseca, S.M. Ransom, P.B. Demorest, Z. Arzoumanian, H. Blumer, P.R. Brook, M.E. DeCesar, T. Dolch, J.A. Ellis et al., Nature Astronomy **4**, 72 (2020), 1904.06759
[41] E. Fonseca, H.T. Cromartie, T.T. Pennucci, P.S. Ray, A.Y. Kirichenko, S.M. Ransom, P.B. Demorest, I.H. Stairs, Z. Arzoumanian, L. Guillemot et al., ApJL **915**, L12 (2021), 2104.00880
[42] M.C. Miller, F.K. Lamb, A.J. Dittmann, S. Bogdanov, Z. Arzoumanian, K.C. Gendreau, S. Guillot, W.C.G. Ho, J.M. Lattimer, M. Loewenstein et al., arXiv e-prints arXiv:2105.06979 (2021), 2105.06979
[43] T.E. Riley, A.L. Watts, P.S. Ray, S. Bogdanov, S. Guillot, S.M. Morsink, A.V. Bilous, Z. Arzoumanian, D. Choudhury, J.S. Deneva et al., ApJL **918**, L27 (2021), 2105.06980
[44] R.W. Romani, D. Kandel, A.V. Filippenko, T.G. Brink, W. Zheng, ApJL **908**, L46 (2021), 2101.09822
[45] T. Dietrich, M.W. Coughlin, P.T.H. Pang, M. Bulla, J. Heinzel, L. Issa, I. Tews, S. Antier, Science **370**, 1450 (2020), 2002.11355
[46] S.M. Couch, C.D. Ott, ApJ **799**, 5 (2015), 1408.1399
[47] D. Radice, C.D. Ott, E. Abdikamalov, S.M. Couch, R. Haas, E. Schnetter, ApJ **820**, 76 (2016), 1510.05022
[48] D. Radice, E. Abdikamalov, C.D. Ott, P. Mösta, S.M. Couch, L.F. Roberts, Journal of Physics G Nuclear Physics **45**, 053003 (2018), 1710.01282
[49] Q.A. Mabanta, J.W. Murphy, ApJ **856**, 22 (2018), 1706.00072
[50] B. Müller, M. Viallet, A. Heger, H.T. Janka, ApJ **833**, 124 (2016), 1605.01393
[51] E. O'Connor, C.D. Ott, Classical and Quantum Gravity **27**, 114103 (2010), 0912.2393
[52] E. O'Connor, ApJS **219**, 24 (2015), 1411.7058

[53] G. Baym, C. Pethick, *Landau Fermi-Liquid Theory: Concepts and Applications* (John Wiley & Sons, Ltd, 1991)